www.sciencemag.org/content/353/6302/919/suppl/DC1

Supplementary Material for

Teleseismic *S* wave microseisms

Kiwamu Nishida* and Ryota Takagi

*Corresponding author. E-mail: knishida@eri.u-tokyo.ac.jp

Published 26 August 2016, *Science* **353**, 919 (2016)
DOI: 10.1126/science.aaf7573

This PDF file includes:

Materials and Methods

Ray-theory Green's function

Here we consider that the vertical displacement of a P-wave detected at a station u_z at a receiver $\mathbf{x}_r$ can be represented by a vertical single force ϕ at $\mathbf{x}_s$ as follows.

$$u_z(\mathbf{x}_r, f) = G(\mathbf{x}_r, \mathbf{x}_s, f)\phi(\mathbf{x}_s, f), \tag{1}$$

where G is the ray-theory Green's function of a P wave (*27, 28*). For a near-vertical propagating P-wave, G can be simplified as,

$$G(\mathbf{x}_r, \mathbf{x}_s, f) = \Gamma \left[\frac{2e^{-2\pi f i T_p - \pi f t^*}}{\pi r^2(\rho_c\alpha_c + \rho_w\alpha_w)} \right] (1 + Re^{-\Phi})^{-1} \sqrt{\frac{dp}{d\Delta}\frac{p}{\sin\Delta}}, \tag{2}$$

where R and Φ are variables for the site amplification via the oceanic reverberation at the source (*7*), ρ_c is the density of crust, ρ_w is the density of water, α_c is the P-wave velocity of the crust, α_w is the P-wave velocity of water, T_p is the P-wave travel time, t^* is the attenuation factor (1 [s]), f is the frequency, p is the ray parameter, Δ is the angular distance between the station and the source, and r is the radius of the Earth. Γ represents the energy loss at the Moho, 410 km and 660 km discontinuities, given by the energy normalized transmission coefficients (*27*) as,

$$\Gamma = \Pi_j \frac{2\sqrt{\rho_j\alpha_j\rho_{j+1}\alpha_{j+1}}}{\rho_j\alpha_j + \rho_{j+1}\alpha_{j+1}}, \tag{3}$$

where ρ_j is the density at the jth layer, and α_j is the P-wave velocity at the jth layer. R and Φ are given by:

$$\begin{aligned} R &= \frac{\rho_c\alpha_c - \rho_w\alpha_w}{\rho_c\alpha_c + \rho_w\alpha_w} \\ \Phi &= \frac{4\pi f h}{\alpha_w}, \end{aligned} \tag{4}$$

where h is the ocean depth at the source.

We inferred the single force by minimizing squared difference between the observations and the synthetic vertical displacement S defined by

$$\sum_i (d_z^i(f) - u_z(\mathbf{x}_r^i, f))^2, \tag{5}$$

where the index i represents station number, and d_z^i is observed vertical displacement. The single force is estimated by

$$\phi(f) = \frac{\sum_i G^*(\mathbf{x}_r^i, \mathbf{x}_s, f) d_z^i(f)}{\sum_i G^*(\mathbf{x}_r, \mathbf{x}_s, f) G(\mathbf{x}_r, \mathbf{x}_s, f)}, \tag{6}$$

where $*$ represents complex conjugate. Because we infer only the vertical single force, the numerator of the above equation is identical to a mathematical formulation of a backprojection method (*24*). The mean squared amplitude of the single force was estimated by integration of the power spectrum from 0.1 to 0.2 Hz.

Equivalent vertical single force to nonlinear forcing by ocean swells

First, we consider a unit cell characterized by correlation length L. The wavenumber-frequency spectrum by the nonlinear forcing of ocean swells can be represented by $F(\mathbf{k}, \omega)$ (*19*) . Forcing to the cell ϕ can be estimated by

$$\phi \equiv \pi L^2 \sqrt{k_c^2 \int F_p(f) df}, \tag{7}$$

where k_c is the cut-off wavenumber $2/L$. The number of cells N within the whole source area S can be written as $N = S/(\pi L^2)$. Assuming that L is smaller than the wavelength of a P-wave, the equivalent vertical single force Φ exerting on the area S can be written by

$$\Phi = \sqrt{N}\phi = 2\pi \sqrt{\int F_p(f) df S}. \tag{8}$$

This result is equivalent to those of previous studies (*29, 30*).

Energy partition between between SH and SV waves by multiple reflections

SV-wave microseisms are converted from P-wave microseisms on the seafloor primarily. Steep bathymetric change is a possible origin of SH-wave microseisms. However, single scattering on the seafloor would be hard to explain the observed ratio between SH-wave and SV-wave amplitudes. During the multiple reflections in the sediment, energy partition between them is expected. In this section, we consider a simplified model for the explanation of the energy partition.

Here we consider SV wave with a unit energy flux enters a flat sedimentary layer with thickness of H [km] (Fig. S3). We assumed that steep topographic changes of the bottom boundary of the sediment caused conversion from SV to SH and that from SH to SV. The energy flux vector $K_n = (K_n^{SV}, K_n^{SH})$ of $n$the reflected S waves can be related to the $(n-1)$th reflection as,

$$\boldsymbol{K_n = A K_{n-1} = A^n K_0} \tag{9}$$

where γ represents conversion coefficient from SV to SH or that from SH to SV, τ represents transmission coefficient from the sedimentary layer to the crust. The matrix A and K_0 are given by

$$\boldsymbol{A} = \begin{pmatrix} \mathbf{1-\gamma-\tau} & \boldsymbol{\gamma} \\ \boldsymbol{\gamma} & \mathbf{1-\gamma-\tau} \end{pmatrix}, \boldsymbol{K_0} = \begin{pmatrix} \mathbf{1} \\ \mathbf{0} \end{pmatrix}. \tag{10}$$

We estimate total energy of transmitted SV and SH wave as,

$$\sum_{\boldsymbol{n=0}}^{\infty} \boldsymbol{\tau K_n} = \begin{pmatrix} \frac{\boldsymbol{\tau+\gamma}}{\boldsymbol{\tau+2\gamma}} \\ \frac{\boldsymbol{\gamma}}{\boldsymbol{\tau+2\gamma}} \end{pmatrix} \tag{11}$$

We define effective path length L by $2H/\tau$, and mean free path l by $2H/\gamma$ (*31*). When the mean free path l is smaller than the effective path length L, energy flux of SH and SV waves are under equipartition state. On the other hand, when l is larger than L, the conversion from SV to SH wave can be neglected.

Resonant frequency of the sediment

For simplicity, we assumed that the upper boundary of sedimentary layer is free surface, whereas the lower boundary is rigid. In this case, the resonant frequency of the fundamental mode can be estimated by $4H/\beta$, where Here β is S-wave velocity of the sedimentary layer and H is the width of the sedimentary layer.

Fig. S1

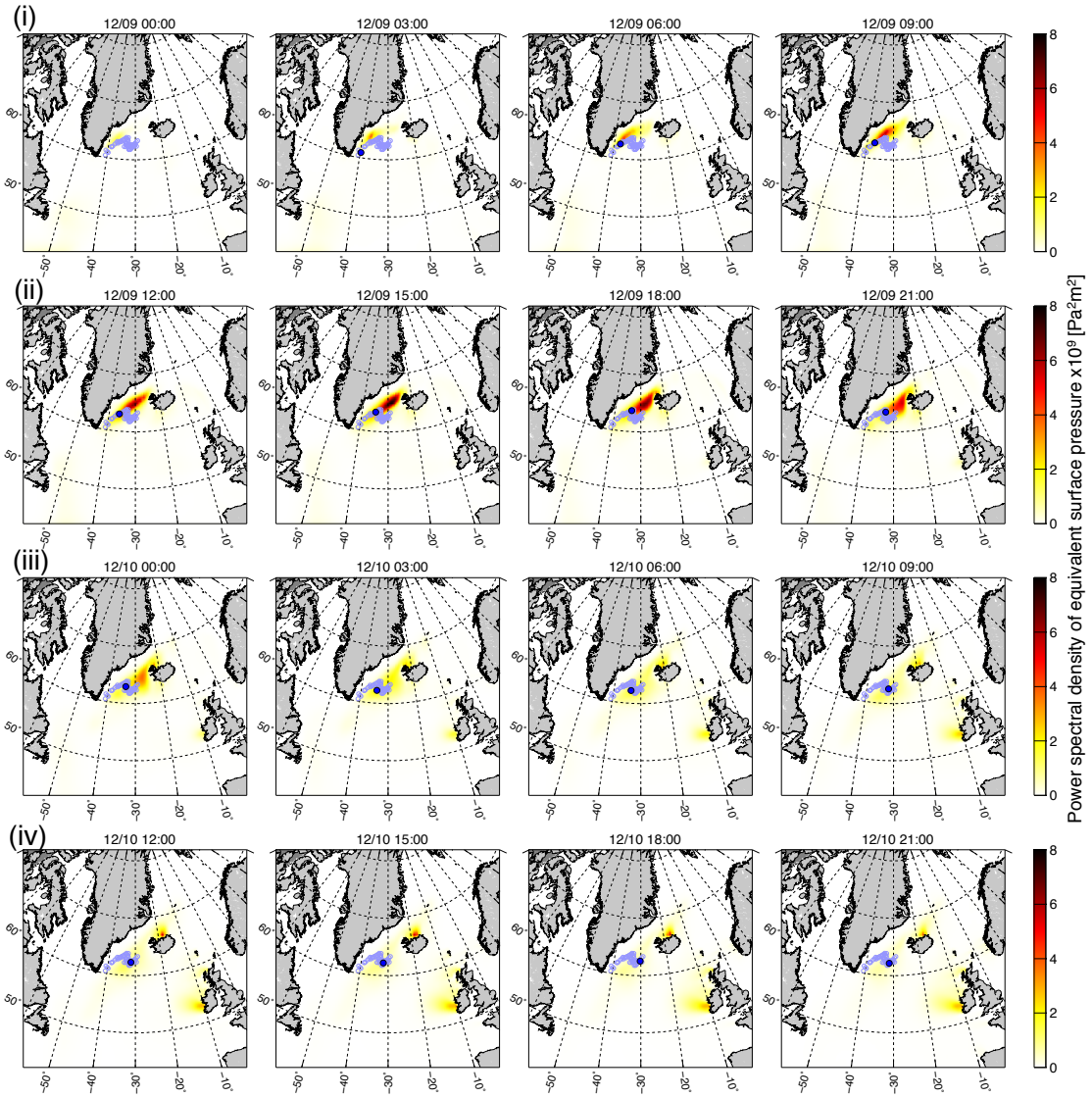

Power spectral density of the wave-induced pressure at the ocean surface based on a numerical wave model WAVEWATCH III (00:00 Dec. 9 to 21:00 Dec. 10, 2014) (*19*). Three-dimensional power spectral density was integrated with respect to the seismic frequency ranging 0.1–0.2 Hz. Each black point shows the estimated centroid location at each time, and the purples ones show all the centroids. (i)–(iv) show time labels every 12 hours shown in Fig. 2A.

Fig. S2

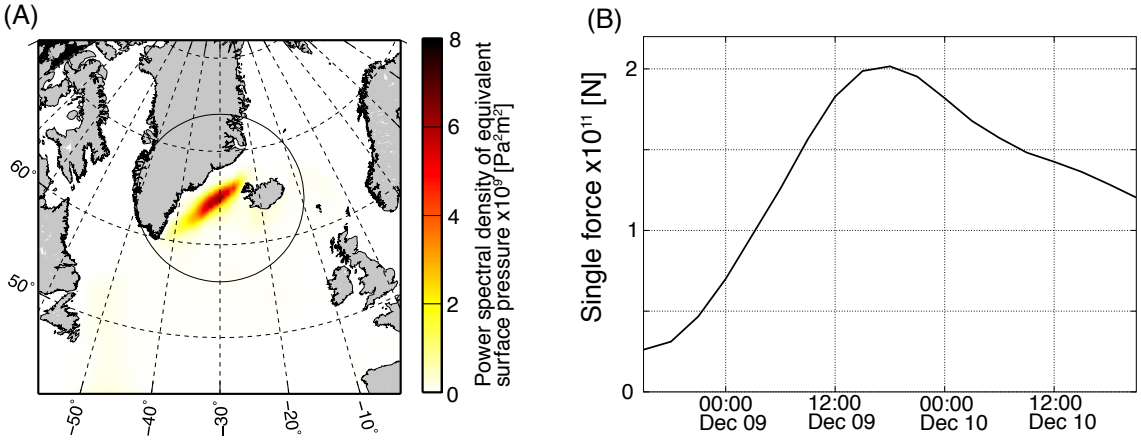

(A) Frequency-integrated power spectral density of the wave-induced pressure at the ocean surface based on the numerical wave model WAVEWATCH III (9 December 2014 12:00 UTC) (*19*). Three-dimensional power spectral density $F_p(f)$ was integrated within a frequency range of 0.1–0.2 Hz. (B) Equivalent single force $2\pi\sqrt{\int F_p(f)df dS}$ (see Materials and Methods for details), where dS is the source area of pressure perturbation. The spatial integration was performed within the circle in (A) for all the time samples.

Fig. S3

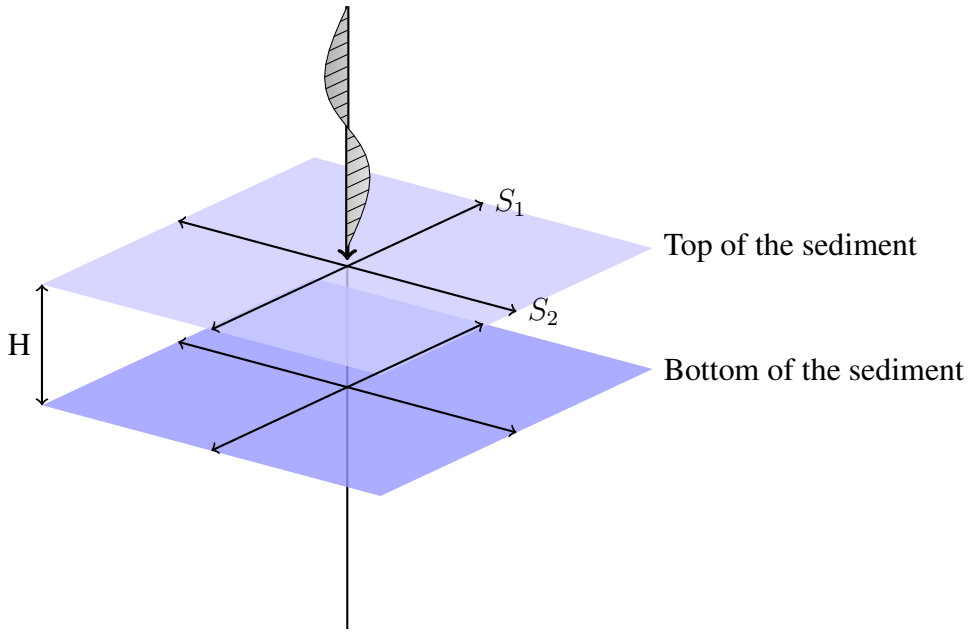

Schematic figure of a simplified model of multiple reflection in a sedimentary layer. S_1 direction corresponds to the polarization direction of incident SV wave, ans S_2 corresponds to SH wave.

References and Notes

1. B. Gutenberg, Microseisms and weather forecasting. *J. Atmos. Sci.* **4**, 21 (1947).

2. R. Snieder, E. Larose, Extracting Earth's elastic wave response from noise measurements. *Annu. Rev. Earth Planet. Sci.* **41**, 183–206 (2013). doi:10.1146/annurev-earth-050212-123936

3. M. S. Longuet-Higgins, A theory of the origin of microseisms. *Phil. Trans. Roy. Soc. A* **243**, 1–35 (1950). doi:10.1098/rsta.1950.0012

4. S. Kedar, M. Longuet-Higgins, F. Webb, N. Graham, R. Clayton, C. Jones, The origin of deep ocean microseisms in the North Atlantic Ocean. *Proc. R. Soc. London Ser. A* **464**, 777–793 (2008). doi:10.1098/rspa.2007.0277

5. P. Gerstoft, M. C. Fehler, K. G. Sabra, When Katrina hit California. *Geophys. Res. Lett.* **33**, L17308 (2006). doi:10.1029/2006GL027270

6. M. Landès, F. Hubans, N. M. Shapiro, A. Paul, M. Campillo, Origin of deep ocean microseisms by using teleseismic body waves. *J. Geophys. Res.* **115** (B5), B05302 (2010). doi:10.1029/2009JB006918

7. L. Gualtieri, E. Stutzmann, V. Farra, Y. Capdeville, M. Schimmel, F. Ardhuin, A. Morelli, Modelling the ocean site effect on seismic noise body waves. *Geophys. J. Int.* **197**, 1096–1106 (2014). doi:10.1093/gji/ggu042

8. Q. Liu, K. Koper, R. Burlacu, S. Ni, F. Wang, C. Zou, Y. Wei, M. Gal, A. M. Reading, A.|Reading, Source locations of teleseismic P, SV, and SH waves observed in microseisms recorded by a large aperture seismic array in China. *Earth Planet. Sci. Lett.* **449**, 39–47 (2016). doi:10.1016/j.epsl.2016.05.035

9. K. Nishida, H. Kawakatsu, Y. Fukao, K. Obara, Background Love and Rayleigh waves simultaneously generated at the Pacific Ocean floors. *Geophys. Res. Lett.* **35**, L16307 (2008). doi:10.1029/2008GL034753

10. F. Ardhuin, L. Gualtieri, E. Stutzmann, How ocean waves rock the Earth: Two mechanisms explain microseisms with periods 3 to 300 s. *Geophys. Res. Lett.* **42**, 765–772 (2015). doi:10.1002/2014GL062782

11. M. N. Toksöz, R. T. Lacoss, Microseisms: Mode structure and sources. *Science* **159**, 872–873 (1968). Medline doi:10.1126/science.159.3817.872

12. L. Vinnik, Sources of microseismic *P* waves. *Pure Appl. Geophys.* **103**, 282–289 (1973). doi:10.1007/BF00876404

13. T. Maeda, K. Obara, T. Furumura, T. Saito, Interference of long-period seismic wavefield observed by the dense Hi-net array in Japan. *J. Geophys. Res.* **116** (B10), B10303 (2011). doi:10.1029/2011JB008464

14. R. Takagi, K. Nishida, Y. Aoki, T. Maeda, K. Masuda, M. Takeo, K. Obara, K. Shiomi, M. Sato, K. Saito, A single bit matters: Coherent noise of seismic data loggers. *Seismol. Res. Lett.* **86**, 901–907 (2015). doi:10.1785/0220150030

15. T. Matsuzawa, K. Obara, T. Maeda, Y. Asano, T. Saito, Love- and Rayleigh-wave microseisms excited by migrating ocean swells in the North Atlantic detected in Japan and Germany. *Bull. Seismol. Soc. Am.* **102**, 1864–1871 (2012). doi:10.1785/0120110269

16. Weather images. *Weather* **70**, 54 (2015). doi:10.1002/wea.2416

17. H. Kawakatsu, On the realtime monitoring of the long-period seismic wavefield. *Bull. Earth. Res. Inst.* **73**, 267–274 (1998).

18. H. L. Tolman, A mosaic approach to wind wave modeling. *Ocean Model.* **25**, 35–47 (2008). doi:10.1016/j.ocemod.2008.06.005

19. F. Ardhuin, E. Stutzmann, M. Schimmel, A. Mangeney, Ocean wave sources of seismic noise. *J. Geophys. Res.* **116** (C9), 1–21 (2011). doi:10.1029/2011JC006952

20. Materials and methods are available as supplementary materials on *Science* Online.

21. B. L. N. Kennett, E. R. Engdahl, R. Buland, Constraints on seismic velocities in the Earth from traveltimes. *Geophys. J. Int.* **122**, 108–124 (1995). doi:10.1111/j.1365-246X.1995.tb03540.x

22. J. VanDecar, R. S. Crosson, B. Y. J. C. Vandecar, R. S. Crosson, Determination of teleseismic relative phase arrival times using multi-channel cross-correlation and least squares. *Bull. Seismol. Soc. Am.* **80**, 150–169 (1990).

23. B. Efron, Bootstrap methods: Another look at the jackknife. *Ann. Stat.* **7**, 1–26 (1979). doi:10.1214/aos/1176344552

24. M. Ishii, P. M. Shearer, H. Houston, J. E. Vidale, Extent, duration and speed of the 2004 Sumatra-Andaman earthquake imaged by the Hi-Net array. *Nature* **435**, 933–936 (2005). Medline

25. G. Laske, G. Masters, Z. Ma, M. Pasyanos, Update on CRUST1.0—A 1-degree Global Model of Earth's Crust, *EGU General Assembly Conference Abstracts* (2013), vol. 15 of *EGU General Assembly Conference Abstracts*, pp. EGU2013–EGU2658.

26. P. Poli, M. Campillo, H. Pedersen, LAPNET Working Group, Body-wave imaging of Earth's mantle discontinuities from ambient seismic noise. *Science* **338**, 1063–1065 (2012). Medline doi:10.1126/science.1228194

27. F. A. Dahlen, J. Tromp, *Theoretical Global Seismology* (Princeton Univ. Press, Princeton, 1998).

28. V. Farra, E. Stutzmann, L. Gualtieri, M. Schimmel, F. Ardhuin, Ray-theoretical modeling of secondary microseism *P*-waves. *Geophys. J. Int.* **206**, 1730–1739 (2016). doi:10.1093/gji/ggw242

29. L. Gualtieri, E. Stutzmann, Y. Capdeville, F. Ardhuin, M. Schimmel, A. Mangeney, A. Morelli, Modelling secondary microseismic noise by normal mode summation. *Geophys. J. Int.* **193**, 1732–1745 (2013). doi:10.1093/gji/ggt090

30. K. Hasselmann, A statistical analysis of the generation of microseisms. *Rev. Geophys.* **1**, 177 (1963). doi:10.1029/RG001i002p00177

31. H. Sato, M. C. Fehler, T. Maeda, *Seismic Wave Propagation and Scattering in the Heterogeneous Earth* (Springer, ed. 2, 2012) pp. 1–494.